A potential role for a novel ZC3H5 complex in regulating mRNA translation in *Trypanosoma brucei*

Received for publication, May 19, 2020, and in revised form, July 29, 2020 Published, Papers in Press, August 5, 2020, DOI 10.1074/jbc.RA120.014346

Kathrin Bajak[1,2], Kevin Leiss[1], Christine Clayton[1], and Esteban Erben[2,*]

From the [1]Zentrum für Molekulare Biologie der Universität Heidelberg (ZMBH), Heidelberg, Germany and [2]Deutsches Krebsforschungszentrum (DKFZ), Heidelberg, Germany

Edited by Karin Musier-Forsyth

In *Trypanosoma brucei* and related kinetoplastids, gene expression regulation occurs mostly posttranscriptionally. Consequently, RNA-binding proteins play a critical role in the regulation of mRNA and protein abundance. Yet, the roles of many RNA-binding proteins are not understood. Our previous research identified the RNA-binding protein ZC3H5 as possibly involved in gene repression, but its role in controlling gene expression was unknown. We here show that ZC3H5 is an essential cytoplasmic RNA-binding protein. RNAi targeting ZC3H5 causes accumulation of precytokinetic cells followed by rapid cell death. Affinity purification and pairwise yeast two-hybrid analysis suggest that ZC3H5 forms a complex with three other proteins, encoded by genes Tb927.11.4900, Tb927.8.1500, and Tb927.7.3040. RNA immunoprecipitation revealed that ZC3H5 is preferentially associated with poorly translated, low-stability mRNAs, the 5′-untranslated regions and coding regions of which are enriched in the motif (U/A)UAG(U/A). As previously found in high-throughput analyses, artificial tethering of ZC3H5 to a reporter mRNA or other complex components repressed reporter expression. However, depletion of ZC3H5 *in vivo* caused only very minor decreases in a few targets, marked increases in the abundances of very stable mRNAs, an increase in monosomes at the expense of large polysomes, and appearance of "halfmer" disomes containing two 80S subunits and one 40S subunit. We speculate that the ZC3H5 complex might be implicated in quality control during the translation of suboptimal open reading frames.

Trypanosoma brucei is a unicellular eukaryote that proliferates in the blood and tissue fluids of mammals and in the digestive system of tsetse flies. *Trypanosoma brucei* and related trypanosomes cause African sleeping sickness in humans and nagana in cattle, diseases which produce a significant economic burden for a vast region of Africa. Two *T. brucei* life-cycle stages are easily cultured in the laboratory. Bloodstream forms (BF) can be grown in high-glucose medium at 37°C, whereas procyclic forms are cultivated in high-proline medium at 27°C.

Kinetoplastids rely almost exclusively on posttranscriptional mechanisms for control of gene expression. Transcription is polycistronic and individual mRNAs are generated by trans splicing of a 39-nucleotide leader to the 5′-end and by 3′ polyadenylation (1). Trypanosome mRNAs vary extensively in decay rates and translation efficiency. Work by numerous laboratories has demonstrated that RNA-binding proteins (RBPs) play prominent roles in the regulation of splicing, translation, and mRNA decay, although the mechanisms by which they do this have, with a few exceptions, remained obscure (1).

Two high-throughput approaches enabled us to identify RBPs that can increase or decrease expression of bound mRNAs. The tethering assay involves co-expression of the protein of interest fused to a highly sequence-specific RNA-binding peptide and a reporter mRNA bearing the cognate recognition sequence; we used the λN peptide–boxB combination. We conducted genome-wide library screens to reveal protein fragments that can either activate or repress expression of a reporter when tethered (2), results that were later verified for a subset of full-length proteins (3). In addition, a catalog of proteins that associate with BF mRNAs (the trypanosome mRNP proteome) was obtained (3). In this method, cells are irradiated with UV light to crosslink proteins to nucleic acids, then polyadenylated (poly(A)$^+$) RNAs are purified via hybridization to oligo(dT) beads under denaturing conditions. The proteins directly bound to poly(A)$^+$ RNAs are then identified and quantified by MS (4). This approach led to the identification of 155 high-confidence RBPs carrying both canonical (RRM, PUF, and zinc finger) and potential novel RNA-binding domains. Although several of the identified RBPs are essential for stage-specific gene expression and/or have developmentally regulated expression or modification (reviewed in Ref. 1), only a small fraction of them exhibited a clear effect on expression when tethered to the mRNA reporter.

One RBP that did have an effect when tethered is a cytoplasmic zinc finger protein named ZC3H5 (Tb927.3.740) (2, 3, 5). ZC3H5 can be crosslinked to, and purifies with, poly(A)$^+$ RNA (3); it decreases gene expression when tethered to a reporter (3). Its expression is similar in multiplying BF and procyclic form trypanosomes, and high-throughput RNAi analysis suggested that it is essential in BF (6). In addition, a yeast two-hybrid screen suggested that ZC3H5 interacts with the de-adenylase CAF1, compatible with the observed repressive activity in the tethering assay (3). In this study, we investigated the role of ZC3H5 in regulating gene expression in *T. brucei*. We found that ZC3H5 is part of a protein

This article contains supporting information.

* For correspondence: Esteban Erben, eerben@iib.unsam.edu.ar.

Present Address for Esteban Erben: Instituto de Investigaciones Biotecnológicas, Universidad Nacional de San Martín (IIBIO-UNSAM)-CONICET, San Martín, Buenos Aires, Argentina.

Present Address for Kathrin Bajak: Center for Integrative Infectious Diseases Research (CIID), Heidelberg, Germany.

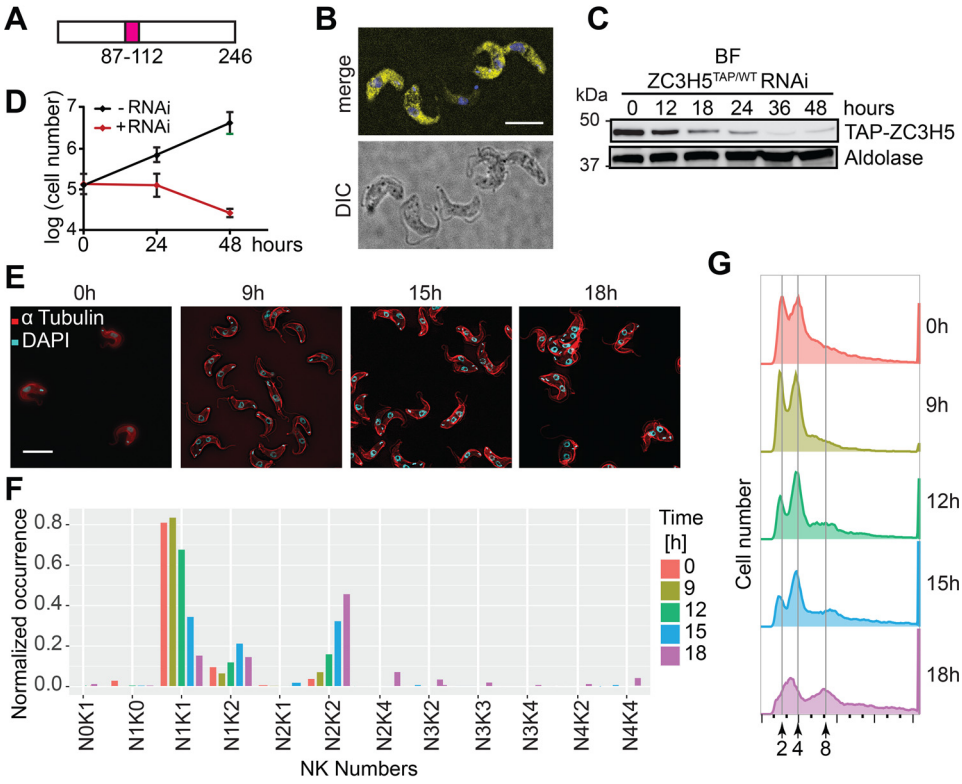

Figure 1. Depletion of ZC3H5 causes accumulation of postmitotic cells. *A*, structure of ZC3H5, to scale. The CCCH zinc finger, as detected by SMART, is shown in *magenta*. *B*, YFP-ZC3H5 is in the cytoplasm. Bloodstream form trypanosomes expressing YFP-ZC3H5 from the endogenous locus were stained for YFP (*yellow*) and for DNA with DAPI (*blue*). Images were examined using the Leica DMi8 spinning disk microscope (*Scale bar*: 10 μM). *C*, disappearance of TAP-ZC3H5 after RNAi. In the cell line used, one copy was *in situ* TAP-tagged and the other was intact. Aldolase served as a control. The numbers of hours after tetracycline addition to induce RNAi are shown. *D*, effect of RNAi on cell numbers. Cumulative cell numbers with and without tetracycline addition are shown for three replicates, with S.D. *E*, effect of ZC3H5 depletion on cell morphology. Cells were stained for DNA (*blue*) and tubulin (*red*). *Scale bar*: 10 μM. *F*, the number of nuclei (N) and kinetoplasts (K) per cell of the population described in (*E*) was quantified ($n > 200$) at the time points indicated. *G*, effect of ZC3H5 depletion on DNA content. DNA was stained with propidium iodide and the cells were analyzed by FACS. The numbers below the diagrams indicate ploidy.

complex which is potentially regulated by GTP binding. RNAi-mediated depletion of ZC3H5 or any other member of the complex results in cells unable to complete cytokinesis. Whereas ZC3H5 preferentially associates with poorly translated, low-stability mRNAs, its depletion results in only minor changes to the transcriptome. We hypothesize that ZC3H5 is involved in quality control during the translation of suboptimal transcripts.

Results

Conservation of ZC3H5 in Kinetoplastea

ZC3H5 is a 25.5-kDa protein with a single C*X*7C*X*5C*X*3H zinc finger domain (Fig. 1*A*). ZC3H5 is present throughout the Kinetoplastea but absent in Euglenids (Fig. S1). Comparison of sequences from *Bodo, Paratrypanosoma, Crithidia, Endotrypanum, Leishmania,* and *Trypanosoma* reveals that the 52 residues surrounding the CCCH domain (5 residues N-terminal, 21 C-terminal) are 51% identical and 81% similar; conservation is stronger if *Bodo* and *Paratrypanosoma* are excluded. The N termini lack charged residues, whereas the C termini are relatively proline-rich. *Paratrypanosoma* ZC3H5 has an 800-residue C-terminal extension. We also verified the cytoplasmic location of ZC3H5, using a cell line with N-terminally *in situ* YFP-tagged protein (Fig. 1*B*).

Depletion of ZC3H5 causes accumulation of precytokinetic trypanosomes

We first confirmed that ZC3H5 is indeed required for BF trypanosome proliferation. To enable detection, we integrated a tandem affinity purification tag sequence (protein A–calmodulin binding peptide) upstream of, and in frame with, one ZC3H5 ORF (TAP-ZC3H5). Induction of RNAi using specific tetracycline-inducible stem-loop dsRNA construct caused a reduction in TAP-ZC3H5 expression within 12 h (Fig. 1*C*) and inhibited cell proliferation (Fig. 1*D*). The phenotype observed upon knockdown of ZC3H5 was also analyzed by fluorescence microscopy (Fig. 1, *E* and *F*) and FACS (Fig. 1*G*). The nuclear and kinetoplastid DNA was stained with DAPI and tubulin staining was used to visualize the cell shape (Fig. 1*E*). After staining for DNA, cells were scored for different cell cycle stages: cells with a single nucleus and kinetoplast (1N1K) are in G_1 or S phase, cells with two kinetoplasts and one nucleus (1N2K) are in G_2 phase, and cells with two kinetoplasts and two nuclei (2N2K) are mitotic or postmitotic. These analyses revealed that the cells were incapable of cytokinesis. Within 18 h of RNAi induction, multinucleate cells were beginning to appear (Fig. 1, *F* and *G*). The DNA profile of cells without RNAi induction suggested the presence of more 4N cells than normal; this perhaps suggests that the cells have somewhat less ZC3H5

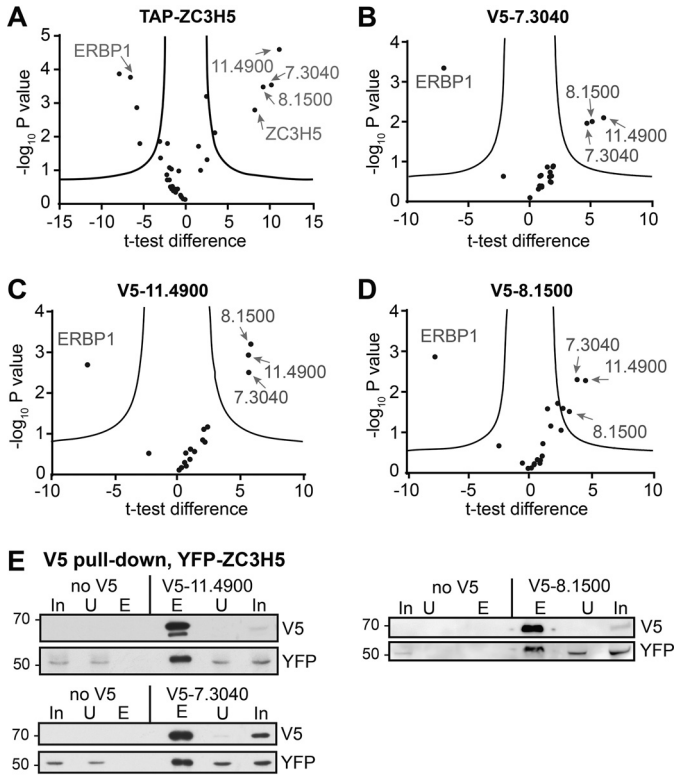

Figure 2. ZC3H5 is associated with three other proteins. *A*, endogenously TAP-tagged ZC3H5 was purified three times. Raw data were analyzed by MaxQuant, and specific interactors were selected from background using label-free quantification in Perseus. In the volcano plots, the ratio of the results with TAP-ZC3H5 to a different TAP-tagged protein, ERBP1, are shown on the *x* axis, and the log10 of the FDR, calculated by a permutation-based FDR adapted *t* test, is on the *y* axis. Significantly selected proteins are labeled (FDR = 0.01, s0 = 2). Gene numbers are truncated by removal of Tb927. Data are in Table S1. *B*, as (*A*) but for V5-Tb927.7.3040. Significantly selected proteins are labeled (FDR = 0.05, s0 = 2). *C*, as (*B*) but for V5-Tb927.11.4900. *D*, as (*B*) but for V5-Tb927.8.1500. *E*, the cells used expressed YFP-ZC3H5 and V5-tagged versions of the interaction partners Tb927.7.3040, Tb927.11.4900, and Tb927.8.1500. After immunoprecipitation the proteins were detected by Western blotting. The eluates are from 10 times more cells than were used for the input and unbound lanes.

than normal. However, the proportion of cells in G_2/M phase increased rapidly upon RNAi induction; this was followed by cell death.

ZC3H5 recruits a protein complex

To examine ZC3H5 interactions, we purified TAP-tagged ZC3H5 and subjected the preparations to MS. To find proteins that were specific to ZC3H5, we compared the results with those from a similar purification of ERBP1 (7), a noncanonical RNA-binding protein that binds to ribosomal protein mRNAs. The results revealed robust copurification of ZC3H5 with the proteins encoded by Tb927.11.4900, Tb927.7.3040, and Tb927.8.1500 (Fig. 2*A* and Table S1). Coprecipitations of the three newly found proteins combined with MS analysis confirmed that they indeed form a complex (Fig. 2, *B–D*). ZC3H5 was however not significantly enriched, suggesting that only a small proportion of 11.4900-7.3040-8.1500 complexes is interacting with ZC3H5. Nevertheless, pulldown of V5 *in situ*–tagged versions of Tb927.11.4900, Tb927.8.1500, and Tb927.7.3040 resulted in clear co-immunoprecipitation of some tagged ZC3H5 (Fig. 2*E*), although most remained in the unbound fraction. The results therefore indicated that a subpopulation of ZC3H5 molecules recruits the Tb927.11.4900-Tb927.8.1500-Tb927.7.3040 complex. All three proteins were in the bloodstream form mRNP proteome (3) (FDR = 0.026, 0.0018, and 0.011, respectively) and are cytoplasmic when fused to GFP (5). MS suggested ZC3H5 interacts also with the RNA-binding protein ZC3H8 (Table S1); however, we did not detect that interaction in co-immunoprecipitation assays (not shown).

Characteristics of the Tb927.7.3040, Tb927.8.1500, and Tb927.11.4900 proteins

We examined the characteristics of the newly identified proteins by comparing the sequences in selected representatives of Trypanosomatida, as well as the more distantly related Kinetoplastid (class Kinetoplastea) *Bodo saltans* (8). Tb927.7.3040 is a 69-kDa protein which has C-terminal WD repeats. It was localized to starvation stress granules in procyclic forms (9) and is conserved as far as *B. saltans* (Fig. S2). The N terminus belongs to the PTHR19924 family, which contains various proteins implicated in rRNA processing.

The 63 kDa Tb927.8.1500 protein is conserved throughout Kinetoplastea (Fig. S3). The sequence alignment reveals three different ~30 residue conserved regions starting at the extreme N terminus and at residues 170 and 262 (*T. brucei* sequence numbers) (Fig. S3). The C-terminal regions are very variable and include proline- and glutamine-rich tracts.

Tb927.11.4900 is absent in *Bodo* but present in Trypanosomatida. It is a 62-kDa protein and contains four WD40 repeats toward the C terminus (Fig. S4). Pro-site scans classify it as being a member of the F-box and WD40 family (PTHR44156), but it lacks an F-box. PTHR44156 includes some guanine nucleotide binding β subunits, and indeed the region of Tb927.11.4900 upstream of the WD repeats includes (in this order) G4, G1, and G3 P-loop NTPase motifs (Fig. 3*A* and Fig. S4). This order is similar to that seen in eukaryotic and prokaryotic circularly permutated GTPases, which have the motif order G4-G5′-G1-G2′-G3 (10, 11). The G4 domain (N/T)K*X*D, which determines specificity for guanine, is present in *T. brucei* Tb927.11.4900 and changed to TK*X*E in other trypanosomes (which should not prevent activity). However, it is less well conserved in other kinetoplastids (Fig. S4). The G1 (P-loop) motif in Tb927.11.4900 has leucine instead of serine/threonine but the lysine required for phosphate interaction is conserved; while the G3 domain (Walker B motif), (D/E)*XX*G, which binds Mg^{2+} and is required for tight nucleotide binding and hydrolysis, is conserved throughout. The G5′ and G2′ motifs are generally poorly conserved and difficult to recognize in primary sequences; G2 has only one threonine totally conserved (11). Threonines are present between the putative G1 and G3 domains in all species examined except *Paratrypanosoma* (Fig. S4).

Interactions between the complex components

To examine interactions between the complex components we used pairwise yeast two-hybrid assays. Unfortunately, ZC3H5 as bait was a constitutive activator preventing its

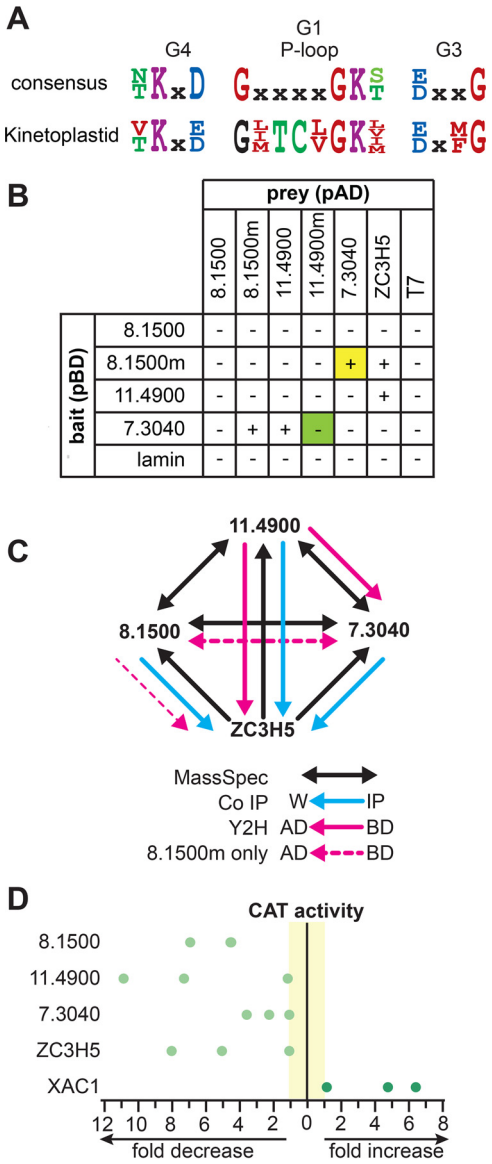

Figure 3. Characteristics and interactions of ZC3H5 complex proteins. *A*, the consensus G4, G1, and G3 sequence motifs as described in Ref. 11 are shown, with the equivalents from Tb927.11.4900 and its homologues. *B*, results from yeast two-hybrid analysis. Plus (+) indicates that the interactions were positive both by growth and α-galactosidase expression. Note that ZC3H5 and Tb927.11.4900m were auto-activators when fused to the DNA-binding domain (not shown). Tb927.8.1500m has a T443E and Tb927.11.4900m has TKVD/AKVA. *C*, summary of interaction studies. The results suggest that Tb927.11.4900 is a central component that interacts with both ZC3H5 and Tb927.7.3040. Tb927.8.1500 interacts with Tb927.7.3040 only when a phosphomimic mutation (T443E) is present in Tb927.8.1500. *D*, all four proteins decrease expression when tethered. Expression of λN-test-protein-myc was induced for 24 h then CAT activity was measured relative to the activity in the absence of induction. Tb927.7.2780 (XAC1) served as a positive control.

evaluation. The results for ZC3H5 as prey, however, suggested that it interacts with Tb927.11.4900. There was also an interaction between Tb927.7.3040 (bait) and Tb927.11.4900 (prey) although the reciprocal interaction was not observed. We concluded that ZC3H5 might recruit Tb927.7.3040 via Tb927.11.4900 (Fig. 3*C*). No interaction of Tb927.8.1500 was observed. However, Tb927.8.1500 has four phosphorylated serines (12, 13) and three phosphothreonines (Fig. S3), one of which, T443, shows peak phosphorylation in late S phase (13). To investigate the effect of the regulated phosphorylation we mutated the relevant threonine (*arrow* in Fig. S3) to aspartate as a phosphomimic. Interestingly, reciprocal interactions were observed between Tb927.8.1500 T443D and Tb927.7.3040, suggesting that full complex formation might be cell-cycle regulated (Fig. 3*B*, *yellow highlight*). However, preliminary co-immunoprecipitation results overexpressing Tb927.8.1500 on a WT background indicated that association of Tb927.8.1500 with ZC3H5 was present in both T443D and T443A mutants (not shown).

To investigate the role of the putative GTP-binding domain in Tb927.11.4900 we mutated the G4 motif, TKVD, to AKVA. In the yeast two-hybrid assay, the resulting protein became constitutively active as bait, but as prey, the interaction with Tb927.7.3040 was lost (Fig. 3*B*, *green highlight*). This raises the possibility that complex formation might depend on Tb927.11.4900 GTP binding.

Tethering of ZC3H5 complex components inhibits reporter gene expression

If the three additional proteins form a complex with ZC3H5, they might all decrease expression when tethered. Previous screening results using random fragments suggested no such activity (2), so we checked the individual full-length proteins. To do this, trypanosomes that constitutively expressed an mRNA encoding the CAT reporter with five boxB elements embedded in its 3′-UTR were transfected with inducible λN fusion proteins. As a positive control, we used XAC1 (Tb927.7.2780). This protein was one of the strongest activators of gene expression in our tethering screens (2, 3), likely caused by its association with translation initiation complexes (14). CAT activity revealed that two of three clones indeed repressed gene expression (Fig. 3*D* and Fig. S6). Consistent with this, results of a preliminary experiment suggested that all four proteins migrate predominantly in the free fractions of a sucrose gradient, rather than with monosomes or polysomes (Fig. S7). However, the association of a minor fraction with monosomes or polysomes cannot be ruled out.

Depletion of ZC3H5 complex components causes accumulation of precytokinetic trypanosomes

We next examined whether the three putative complex components were required for cell proliferation. In each case, we used cells in which one copy of the relevant gene had an *in situ* V5 tag at the N terminus. RNAi against any of the three proteins prevented proliferation and caused accumulation of cells with 4N, and then >4N DNA content, indicating defective cytokinesis (Fig. 4). In each case also, the culture recovered as cells without RNAi were selected. Loss of each protein therefore had an effect similar to that seen after ZC3H5 depletion.

ZC3H5 mRNA binding

To further examine the function of ZC3H5, we pulled down TAP-ZC3H5, released the RNA-protein complexes by TEV protease cleavage, and sequenced RNA from both bound and

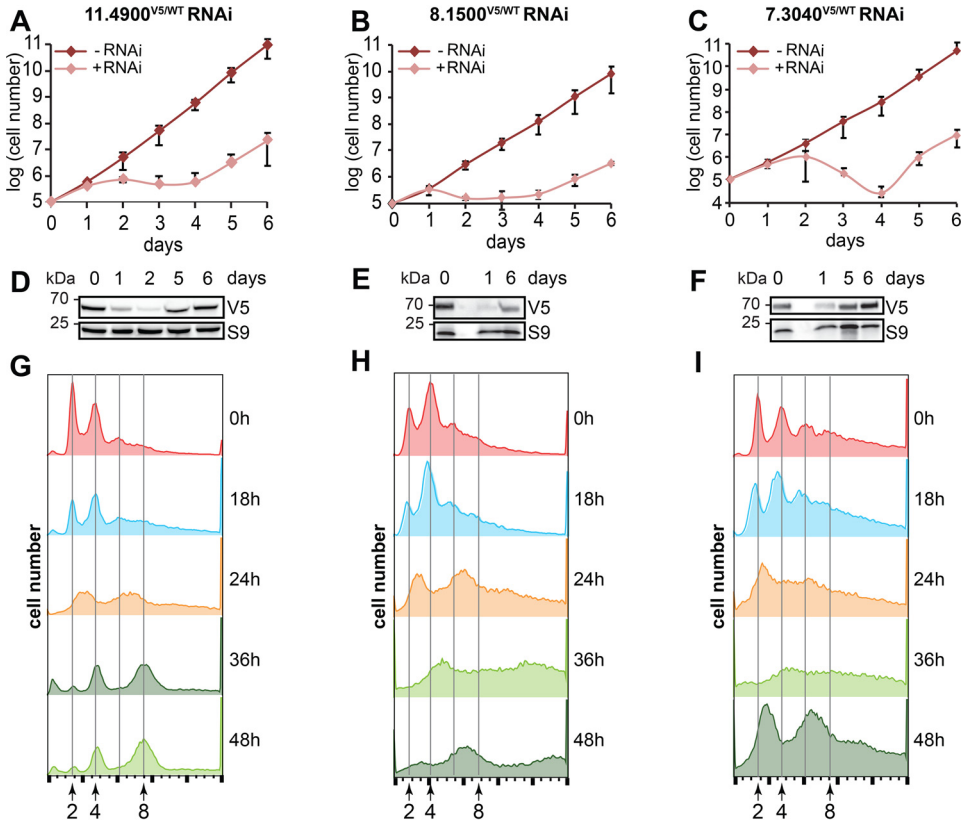

Figure 4. Effects of depleting ZC3H5 interaction partners. *A–C*, effects of depletion on cell growth. Cumulative cell numbers with and without tetracycline addition are shown for three replicates, with S.D. *D–F*, disappearance (and reappearance) of V5-tagged proteins after RNAi. In the cell line used, one copy was *in situ* V5-tagged and the other was intact. S9 served as a control. The numbers of days after tetracycline addition to induce RNAi are shown. *G–I*, effect of protein depletion on DNA content. DNA was stained with propidium iodide and the cells were analyzed by FACS. The numbers below the diagrams indicate ploidy.

unbound (flow-through) fractions. Principal component analysis (Fig. S8*A*) demonstrated clear separation of the bound and unbound fractions. The *ZC3H5* mRNA was more than 20-fold enriched in the bound fractions, consistent with selection via the nascent polypeptide (Table S2, *sheet 1*). The trypanosome genome contains many repeated genes; if these are all counted, they can bias analysis. We therefore considered only a list of unique genes (15). Also, because mRNAs encoding ribosomal proteins are exceptionally short and behave abnormally in a variety of ways, they were omitted from the subsequent statistical analyses (see Figs. 5 and 7). There was a moderate correlation between binding and mRNA length (Fig. 5*A* and Fig. S9).

We now compared the 184 mRNAs that were at least 4-fold enriched with a similar number of mRNAs that were least enriched (again excluding ribosomal protein mRNAs). (The compared genes are listed in Table S2, *sheet 4*; the least enriched set was at least 3.8-fold more abundant in the unbound than in the bound fraction.) The enriched mRNAs were significantly longer than the depleted mRNAs (Fig. 5*A*), suggesting a degree of nonspecificity in the selection. To find motifs that are enriched in bound mRNAs, the 5′-UTRs, 3′-UTRs, and coding regions were compared separately. Most of the 5′-UTRs are annotated but only 60% of mRNAs have annotated 3′-UTRs. For all three comparisons, there was significant enrichment of motifs including the sequence UAG (Fig. 5*B*). However, this might have been an artifact because the average sequence lengths examined from the bound fraction were 1.6-fold (UTRs) and 2.6-fold (coding regions) longer than those from the unbound fraction (Fig. 5*A*). We therefore compared a manually selected subset of bound and unbound coding regions that were as closely length-matched as possible (this resulted in 98 matched mRNAs; see Table S2, *sheet 4*). Enrichment of (U/A)UAG(A/G) persisted (Fig. 5*B*), suggesting that ZC3H5 indeed preferentially selects mRNAs containing the motif. The enriched mRNAs had the same stop codon distribution as the nonenriched set, suggesting that the additional UAGs were not in frame.

We next looked at the biological characteristics of the bound mRNAs. Comparison of the bound and unbound sets revealed a statistically significant preference for association with mRNAs with shorter half-lives (Fig. 5*A*). Notably, there were no mRNAs with half-lives above 120 min in the ZC3H5-bound fraction (Fig. S9*B*). The correlation between binding and ribosome occupancy was probably too weak to be meaningful (Fig. S9, *C* and *D*, and Fig. 5*A*). There were no significant differences in ORF codon optimality (Fig. 5*A*) between bound and unbound RNAs. About 6% of both the bound and the unbound mRNAs have upstream open reading frames, arguing against a role for these in ZC3H5 association. When we examined functional classes, however, there was clear preferential binding of mRNAs from genes that are related to PAG genes (Fig. 6*A*). PAG genes (procyclin-associated genes)

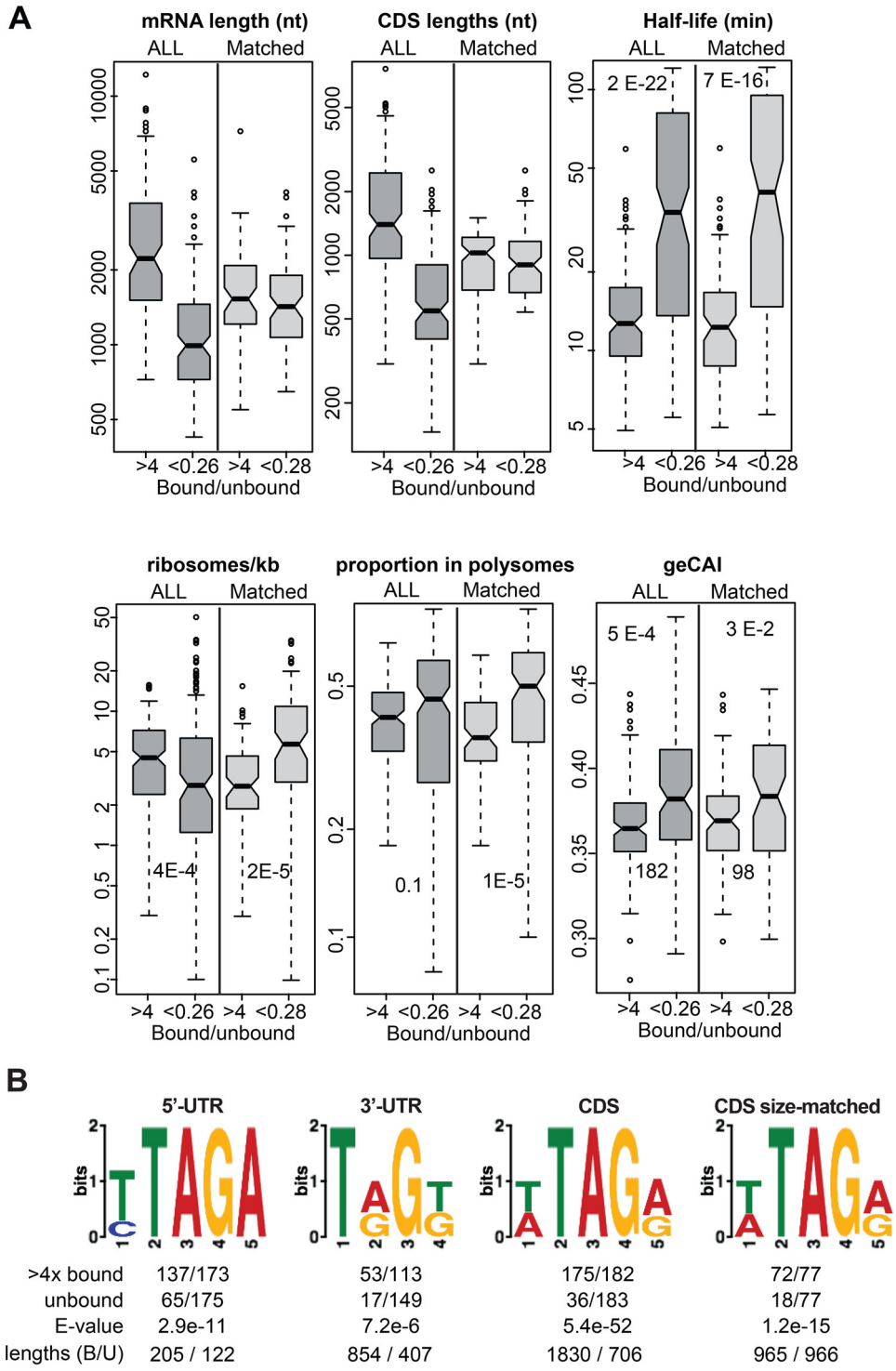

Figure 5. Binding of mRNAs by ZC3H5. *A*, comparison of bound and unbound mRNAs. The 182 bound mRNAs that showed at least 4-fold enrichment were compared with the 182 mRNAs that showed least binding, after exclusion of mRNAs encoding ribosomal proteins. These are labeled *ALL* in the plots. To eliminate possible bias caused by length differences, 98 mRNAs were selected from both sets to obtain matched distributions of coding region lengths; these results are labeled *Matched*. The genes concerned are listed in Table S2, *sheet 4*. Half-lives are from Ref. 48, ribosome densities are from Ref. 49, the proportion in polysomes is from this paper, and the geCAI values are from Ref. 32. Values for all genes are shown as scatter plots in Fig. S7. *B*, motifs enriched in the bound mRNAs as compared with the unbound mRNAs as in (*A*). 5′-UTRs, 3′-UTRs, and coding sequences (*CDS*) were considered separately; some UTRs are not annotated. *>4× bound* and *unbound* show the number of sequences containing the motif relative to the total number considered. The E-value is from DREME. The median lengths of the sequences considered are shown at the bottom, with bound first and unbound second. Results for the matched CDSs are shown on the far right.

were originally found downstream of, and cotranscribed with, the genes encoding the major procyclic surface proteins, the procyclins (16). There are however various other PAG orthologues that are transcribed by RNA polymerase II, are easily distinguished from the procyclin-associated genes at the DNA sequence level, and are well expressed in

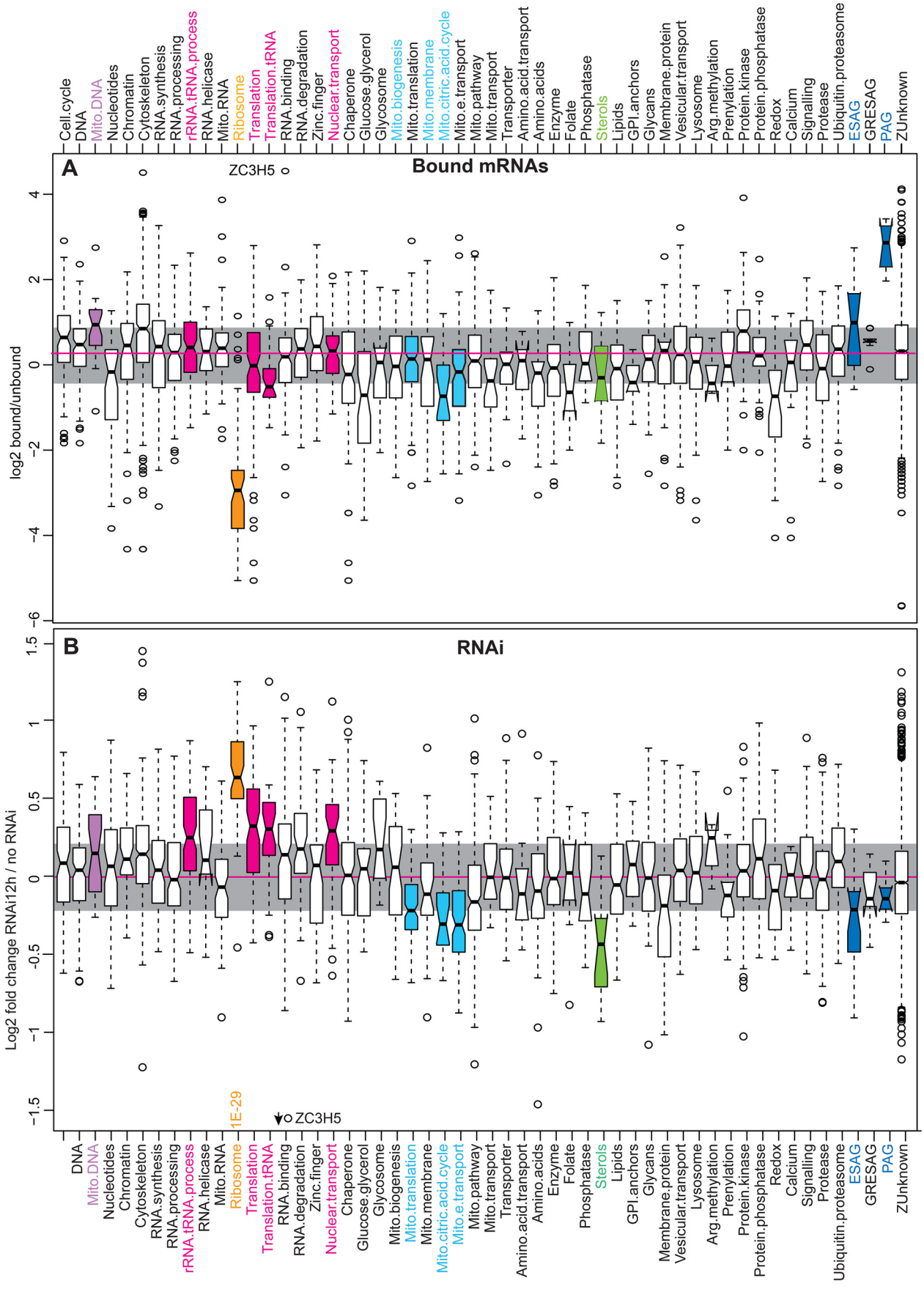
A
Bound mRNAs
ZC3H5
log2 bound/unbound
B
RNAi
Log2 fold change RNAi12h / no RNAi
ZC3H5
1E-29
Cell.cycle
DNA
Mito.DNA
Nucleotides
Chromatin
Cytoskeleton
RNA.synthesis
RNA.processing
rRNA.tRNA.process
RNA.helicase
Mito.RNA
Ribosome
Translation
Translation.tRNA
RNA.binding
RNA.degradation
Zinc.finger
Nuclear.transport
Chaperone
Glucose.glycerol
Glycosome
Mito.biogenesis
Mito.translation
Mito.membrane
Mito.citric.acid.cycle
Mito.e.transport
Mito.pathway
Mito.transport
Transporter
Amino.acid.transport
Amino.acids
Enzyme
Folate
Phosphatase
Sterols
Lipids
GPI.anchors
Glycans
Membrane.protein
Vesicular.transport
Lysosome
Arg.methylation
Prenylation
Protein.kinase
Protein.phosphatase
Redox
Calcium
Signalling
Protease
Ubiquitin.proteasome
ESAG
GRESAG
PAG
ZUnknown

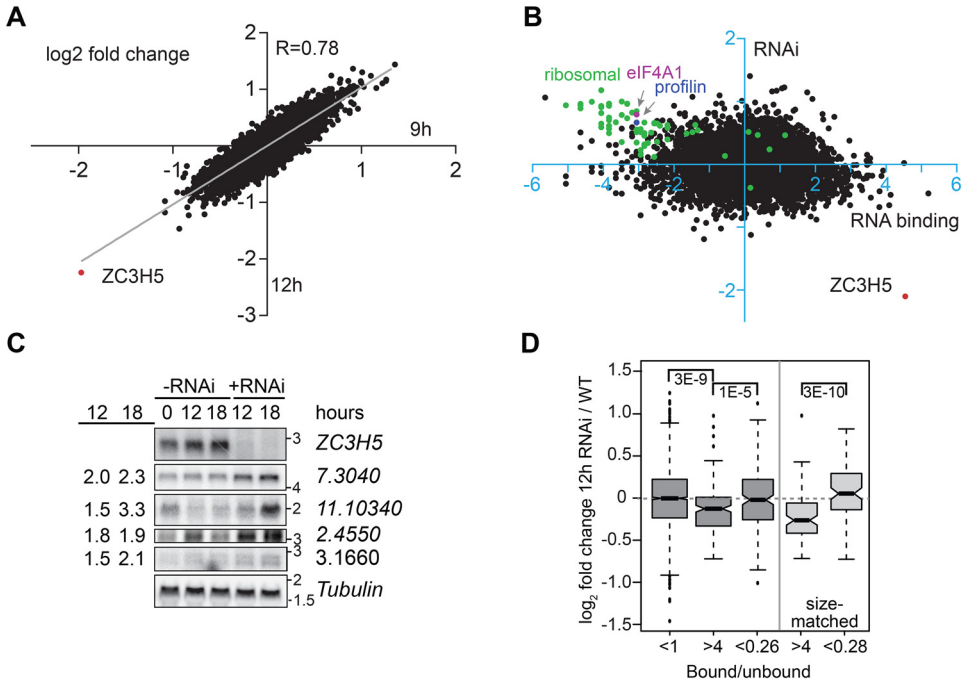

Figure 7. Effects of depleting ZC3H5 on the transcriptome. RNAi was induced in duplicate cultures of bloodstream form trypanosomes for 9 or 12h, then RNA was analyzed by RNA-Seq. Results for a set of coding regions representing all unique genes are shown. -Fold changes relative to duplicate uninduced cultures were calculated using DeSeq2 (45). *A*, log2 -fold changes, relative to control, after 9 and 12 h RNAi, calculated using DeSeq2. Each spot represents a single mRNA. *B*, the average RNA binding ratio is on the *x* axis and log2 -fold changes, relative to control, after 12 h RNAi on the *y* axis. All values are log2 transformed. *C*, Northern blotting confirming increases in four mRNAs after ZC3H5 RNAi. Tubulin serves as a control. The numbers on the *left* indicate the signal intensity after 12 or 18 h of RNAi, divided by the average signal intensity for cells grown without tetracycline, normalized to the tubulin control. *D*, effects of RNAi on mRNAs classified according to ZC3H5 binding. The *box plot* shows the median with 25th and 75th percentiles. *Whiskers* extend to the furthest point within 1.5-fold the interquartile range, and dots are outliers. Less than 1 (<1) are all mRNAs with a maximal binding ratio of less than 1 in both replicates; >4 are the 183 mRNAs with a minimal binding ratio of 4 in both replicates. Less than 26 (<0.26) are the 183 mRNAs that showed lowest binding, excluding mRNAs that encode ribosomal proteins. The size-matched datasets (*lighter gray fill*) are 98 lowest-binding mRNAs selected such that their coding region lengths match those of 98 mRNAs that showed >4 times binding (see Table S2). Results of pairwise *t* tests are shown above the boxes.

bloodstream forms. Seven PAG genes are included in the set of unique genes and mRNAs from all of them were enriched in the ZC3H5-bound fraction. Scrutiny of transcriptome data, as well as some Northern blot data for one of the relevant genes (17), suggested that these mRNAs are mostly less than 2-kb long, so they were not selected because they are inordinately long. Each of the open reading frames has at least three copies of the potential (U/A)UAG(A/G) motif. As an independent verification of the motif we looked for it in the open reading frames encoding ribosomal proteins, because these had been excluded from the motif search. These sequences comprise, in total, over 32 kb. From their base composition, and allowing for the absence of in-frame UAG stop codons in open reading frames, over 70 (U/A)UAG(A/G) motifs would be expected. However, only two of the coding regions contain the motif. In agreement with this observation, ribosomal encoding transcripts were the most underrepresented functional category in the bound fraction (Fig. 6*A*).

Effects of ZC3H5 depletion on the transcriptome and translation

Because reporter expression is inhibited by tethered ZC3H5, we expect its depletion to increase the abundance and/or translation of bound mRNAs. We tested this by characterizing the transcriptomes of parasites after 9 and 12 h RNAi (Table S2). These two time points were chosen because the cytokinesis defect was just beginning to be apparent by 12 h and we hoped to avoid secondary effects. We compared the results with those from WT cells because the uninduced cells already had a slightly unusual cell cycle profile (Fig. 1). Principal component analysis showed good separation of the samples (Fig. S8*B*) and ZC3H5 mRNA was significantly decreased at both time points (Fig. 7*A* and Table S2). Moreover, results from 9 and 12 h RNAi

Figure 6. mRNAs associated with ZC3H5 and effects of ZC3H5 depletion in particular functional classes. *A*, the average of bound/unbound RNA for both replicates was calculated. All mRNAs were classified according to their protein function, where known, as in Table S2. The ratios for each class are shown as *box plots*. *Central line*: median; upper, and lower limits are 75th and 25th percentiles; *Whiskers* extend to the furthest measurement up to 1.5 times the interquartile range, and *circles* are outliers. The *shaded region* shows the overall interquartile range, and the overall median is in *magenta*. The ribosome class (significantly depleted by ANOVA, $p = 0.0009$) is in *brown* and three classes that had medians above the overall 75th percentile are in *cyan*; only the PAG class is significantly enriched ($p = 0.02$). *B*, the -fold changes on mRNA after 12 h RNAi were calculated using DESeq2. All mRNAs were classified according to their protein function, where known, as in Table S2. The ratios for each class are shown as *box plots*. *Central line*: median; upper and lower limits are 75th and 25th percentiles; *whiskers* extend to the furthest measurement up to 1.5 times the interquartile range; and *circles* are outliers. The *shaded region* shows the overall interquartile range and the overall median is in *magenta*. The ribosome class (significantly increased by ANOVA, P = 1E-29) is in *brown* and other classes are colored if they have medians above the overall 75th percentile (*pink*) are or below the 25th percentile (mitochondrial in *cyan*, sterol metabolism in *green*). ANOVA *p*-values are indicated.

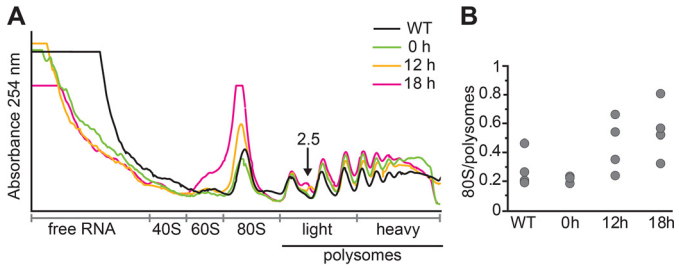

Figure 8. Effects of depleting ZC3H5 on polysomes. Ribosomes and polysomes were separated on sucrose gradients, after 12 h, 18 h RNAi, or without RNAi (0 h). Because RNAi is leaky, the parental cell line was also included. *A*, the absorbance at 254 nm (random units) is shown for one experiment. The *arrow* points to the additional 2.5× peak after RNAi; it suggests a defect in commencing elongation. *B*, quantitation of the ratio between the 80S and polysome 254 nm measurements for four independent experiments.

correlated well, with slightly increased effects at 12 h (Fig. 7*A*). Most of the significant changes were, however, extremely small (1.5- to 2-fold) (Fig. 7, *A* and *B*). Although we confirmed four of them by Northern blotting, with increased effects at 18 h (Fig. 7*C*), interpretation of such small effects is difficult. Unexpectedly, ZC3H5-bound mRNAs were mostly slightly (but not significantly) decreased whereas, as expected, unbound mRNAs were, on average, unaffected (Fig. 7*D*). The most marked and significant effects were increases in mRNAs encoding ribosomal proteins, which were the least bound class (Figs. 6, *A* and *B*, and 7*B*).We also looked at the proportions of each mRNA that are associated with polysomes in WT cells, using data from Table S3 (see below). The mRNAs that increased were significantly more polysome-associated than those that decreased; which is in accordance with their longer half-lives (translation is known to influence the mRNA $t_{1/2}$) Interestingly, there were significant but small increases (FDR = 0.05, >1.5-fold) in mRNAs encoding five components of the Tric complex, five translation factors, six RNA-binding proteins and two components of the CAF1-NOT complex. Overall, the data suggested slight up-regulation of mRNAs encoding the translation machinery (Fig. 6*B*).

Because the results from total mRNA were somewhat paradoxical, we wondered whether translation was selectively affected. We therefore examined the effect of *ZC3H5* RNAi on the polysomal distribution of mRNAs, subjecting extracts to sucrose gradient centrifugation. The polysome profiles were altered, with an increase in monosomes at the expense of the heaviest polysome fractions (Fig. 8, *A* and *B*; another example in Fig. S10, *A–C*, *upper panels*). A similar change is seen in stumpy form trypanosomes (18) but the transcriptome changes upon ZC3H5 depletion showed no correlation with those seen during stumpy form differentiation (Fig. S10*D*).

To find out whether specific mRNAs had moved into the monosome fraction after ZC3H5 depletion, we sequenced the mRNAs in free, monosome, light polysome (2, 3, and 4 ribosomes) and heavy polysome (>4 ribosomes) fractions. This analysis can show major movements of mRNAs between non-translated and translated fractions but is too insensitive to detect more subtle alterations. Movement of *ZC3H5* mRNA from the polysome fractions to the free fraction was indeed clearly demonstrated (Fig. S8*C*). However, the principal component analysis suggested no significant changes in mRNA distributions between the fractions after RNAi (Fig. S8*D*). Some statistically significant differences for some mRNAs in the free fractions (Table S3) can be ignored because they were for mRNAs that were predominantly in the other fractions. Otherwise, no significant differences were seen. These results suggest that the increase in monosomes probably represented free ribosomes. Despite this, there was no effect on the total mRNA amount (Fig. S11*A*) or on the overall protein synthesis pattern, at least for the more strongly translated mRNAs (Fig. S11*B*).

Interestingly, the polysome profiles of ZC3H5-depleted trypanosomes had a clear new peak at the 2.5 position. Halfmers in polysome profiles consist of one or more full ribosomes plus a 40S subunit (19), and they arise when there are problems with 60S subunit joining. One possible cause is defective large subunit biogenesis (20). In trypanosomes, defects in ribosome biogenesis and export from the nucleus can cause feedback inhibition of rRNA processing (21–23). A role of the ZC3H5 complex in ribosome biogenesis seemed unlikely, given its cytoplasmic location, and indeed, ZC3H5 depletion had no reproducible effect on the overall pattern of rRNAs and precursors (Fig. S12).

Discussion

The regulation of gene expression in trypanosomatids occurs mainly at the posttranscriptional level; thus, RNA-binding proteins are fundamental for the regulation of mRNA and protein abundance. Our studies showed that the RNA-binding protein ZC3H5 is conserved in the Kinetoplastea, it localizes in the cytoplasm and is essential for cell growth. We demonstrated that it associates with three other previously uncharacterized proteins, encoded by genes Tb927.11.4900, Tb927.8.1500, and Tb927.7.3040, but not with components of the de-adenylation NOT complex. Initial attempts to identify the factors that recruit the de-adenylase CAF1 to its mRNA targets, suggested ZC3H5 to be one of the linking proteins between the mRNA and the degradation complex (3). However, neither CAF1 nor any other component of the NOT1 complex was detected in our MS analysis. Nevertheless, ZC3H5 copurifies with three other proteins and our results suggest that they act as a complex. Each one inhibits expression when tethered in the 3′-UTR of a reporter mRNA, and depletion of any one of the four subunits causes the same phenotype, the accumulation of postmitotic cells.

Pairwise yeast two-hybrid analysis suggests that ZC3H5 might recruit Tb927.7.3040 via Tb927.11.4900 and that the interaction between the last two proteins may be GTP-dependent. Mutation of the Tb927.11.4900 GTP-binding domain prevented interaction with the Tb927.7.3040. These analyses also suggested that Tb927.8.1500 form part of the complex only when it is phosphorylated in T443, a modification that peaks in late S phase (13). However, we do not know yet whether these modifications regulate the dynamics of complex formation *in vivo*. It is apparent that, at least under the conditions investigated, most ZC3H5 molecules are not associated with the identified complex. Because these proteins were found to be associated to poly(A)$^+$ RNA (3), it seems plausible that ZC3H5 brings

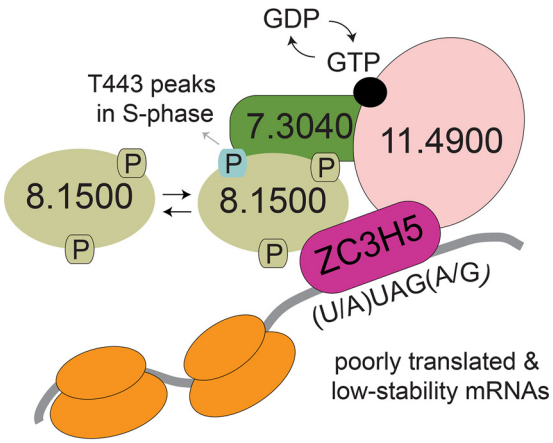

Figure 9. A possible mechanism for mRNA quality control by ZC3H5 in bloodstream forms. For example, ZC3H5 is bound to (U/A)UAG(U/A) motifs on the mRNA and recruits a protein complex. Complex formation is assisted by GTP-GDP exchange on Tb927.11.4900 and cycling phosphorylation status on Tb927.8.1500. Only a fraction of ZC3H5 is associated with these complexes (not shown).

the complex components into close proximity to mRNA (Fig. 9). The associated proteins might also complement the ZC3H5-binding interface, for instance through the low complexity regions present on Tb927.8.1500, increasing target affinity.

Tb927.11.4900 protein has a circularly permuted GTPase domain. Previously characterized eukaryotic (nonorganellar) proteins with this domain arrangement, typified by yeast Noa1, Lsg1, Gnl1, Gnl2, and Gnl3l (24), are mostly in the nucleolus and are implicated in ribosome biogenesis (25). These proteins are conserved in eukaryotic evolution and homologues are indeed present in trypanosomes. Because of its cytoplasmic location (5), Tb927.11.4900 is unlikely to have a role in nuclear ribosome biogenesis, but it (or the complete complex) might be implicated in cytoplasmic ribosome maturation or modification.

Loss of ZC3H5 caused a slight decrease in very heavy polysomes, and an increase in monosomes. It is normally assumed that 80S ribosomes dissociate into their component subunits upon translation termination. If this were universally true, the 80S peak would represent mRNAs bearing a single ribosome each. Indeed, in growing *Saccharomyces cerevisiae*, most 80S ribosomes are elongating (26). Free monosomes have, however, been observed in mammalian cells subject to ribotoxic stress (27). An increase in monosomes, but not 2.5 mers, is seen in stumpy form trypanosomes (18). Because these also show a strong decrease in mRNA levels, it seems likely that free 80S subunits are present. We observed no movement of mRNAs toward the monosome fraction in ZC3H5-depleted cells, so we suggest that their monosomes are not associated with mRNAs. It is impossible to tell whether this is a direct effect of ZC3H5 depletion or a secondary symptom of the onset of growth inhibition.

The appearance of 2.5 mers in ZC3H5-depleted cells is a much more specific defect and has not been observed previously in trypanosomes. In budding yeast, halfmers were first seen after treatment with low concentrations of cycloheximide (19), with clear peaks at the 1.5, 2.5, 3.5, and 4.5 mer positions. Halfmers were also seen after depletion of proteins required for ribosome biogenesis, export, cytoplasmic maturation, or translation initiation (20, 28–31); they indicate a failure of 60S ribosomal subunit joining. In ZC3H5-depleted cells, however, the only increase detected was in 2.5 mers, arguing against a general late ribosome biogenesis defect. The 2.5 mers could consist of one ribosome on the start codon, a second 80S ribosome immediately downstream of the first and a 40S subunit queueing behind them in the 5′-UTR. This could be caused by a newly initiated ribosome failing to continue elongation. The coding regions and 5′-UTRs of mRNAs that bound to ZC3H5 were enriched in the motif [U/A]UAG[U/A]. Because UAG is a stop codon, this suggests an increased presence of four codons that specify amino acids: [U/A]UA (perhaps followed by G) and AG[U/A] (perhaps preceded by U). Comparison of the first 60 coding nucleotides of the 182 bound mRNAs (4×) with the same number of least enriched mRNAs still showed significant (1.1E-7) enrichment of UAG, present in 80 of the bound but only 22 of the unbound mRNAs. Using the codon optimality indices calculated in Ref. 32, the codons *X*UA and AG*X* are, on average, suboptimal (Fig. S13).

After ZC3H5 depletion, the vast majority of bound mRNAs showed no change in abundance, and a few decreased. This is the reverse of the effect that would be expected if the ZC3H5 complex suppresses expression. We therefore suspect that the tethering results are misleading. This could be because the complex does not work in the normal way when attached to the 3′-UTR, or because its effects are dependent on the nature of the ORF. We know that slow translation elongation can favor correct folding of proteins that are prone to aggregation (33), and therefore more active product than when translation is faster. However, so far as we know, the failure of a protein to fold does not normally result in a decrease in the amount of the encoding mRNA. We propose, instead, that the codon composition of the reporter influences the effect of ZC3H5 complex binding. This is suggested by the fact that motifs associated with ZC3H5 binding are enriched in the coding region. In yeast, increases in the initiation rate have different effects on translation depending on the codon optimality of the ORF (34). If the coding region is easily translated, increasing the initiation rate will increase the translation rate. In contrast, if there are clusters of suboptimal codons, increasing the initiation rate will lead to ribosome collisions, which result in premature termination and RNA cleavage by the quality control machinery (34). Thus, a complex that decreases translation of an optimal ORF might actually enhance translation of an ORF with suboptimal codons (Fig. 9).

In summary, we propose that the ZC3H5 complex is implicated in quality control during the translation of suboptimal open reading frames, and that its assembly may be regulated by a GTP-GDP hydrolysis and exchange cycle.

Experimental procedures

Cells and plasmids

All experiments were done with Lister 427 monomorphic bloodstream form parasites expressing the Tet-repressor. Parasites were cultivated in HMI-9 medium in an incubator at 37°C

with 5% CO_2. Stable cell lines were made with *in situ* TAP-, V5-, or YFP-tagged ORFs. Most of the plasmids were assembled using the NEBuilder HiFi DNA Assembly Master Mix (New England Biolabs) following manufacturer's recommendations. RNAi target gene fragments were selected based on default settings of the RNAit software (35). They were amplified from genomic DNA using primers with a 5′ extension including *attB* sites for cloning into the stem loop pGL2084 plasmid (36). The resulting plasmid was digested with BamHI and HindIII and the fragment containing the stem loop was subcloned into the pHD1146 plasmid. For the tethering assays, cell lines constitutively expressing CAT reporter with boxB actin 3′-UTR were cotransfected with plasmids encoding Tb927.8.1500, Tb927.7.3040, and Tb927.11.4900 in fusion with the λN-peptide (2, 3). Stable transfectants were selected in the presence of appropriate selective drugs at the following concentrations: 1 μg ml^{-1} puromycin, 2.5 μg ml^{-1} phleomycin (InvivoGen), 5 μg ml^{-1} hygromycin B (Calbiochem), and 10 μg ml^{-1} blasticidin (InvivoGen) and independent clones obtained by limiting dilution. For yeast two-hybrid, all entry clones were shuttled into the Gateway-compatible vector (37) and pairwise analysis performed as previously described (3). The Tb927.8.1500 and Tb927.11.4900 mutants were generated using the Q5 Site-Directed Mutagenesis Kit (New England Biolabs) from the WT vector templates. Details of all plasmids and oligonucleotides are found in Table S4.

Protein analysis

Proteins were analyzed by Western blotting and detected by enhanced chemiluminescence according to the manufacturer's instructions (Amersham Biosciences). Antibodies were against the V5 tag (AbD seroTec, 1:1000), the YFP tag (Roche, 1:1000), and aldolase (rabbit, 1:50,000). CAT was measured in a kinetic assay involving partition of ^{14}C-buturyl chloramphenicol from the aqueous to the organic phase of scintillation fluid (38). Co-immunoprecipitations of endogenously V5-tagged ERBP1 (7), Tb927.8.1500, Tb927.7.3040, and Tb927.11.4900 proteins were done as previously described (39). Tandem affinity purification of *in situ* TAP-tagged ZC3H5 was essentially carried out according to Mugo and Clayton (40).

Quantitative MS data analysis

Purified proteins were separated on SDS 4 to 20% polyacrylamide gradient gels (Bio-Rad) and stained by colloidal Coomassie Blue. Copurified proteins were analyzed in three independent biological experiments by LC-MS by the ZMBH Mass Spectrometry facility via the Ultimate 3000 liquid chromatography system directly coupled to an Orbitrap Elite mass spectrometer (Thermo Fisher). Samples were delivered to an in-house packed analytical column (inner diameter 75 μM × 20 cm; CS-Chromatographie Service GmbH, Langerwehe, Germany) filled with 1.9 μM ReprosilPur-AQ 120 C18 material (Dr. Maisch, Ammerbuch-Entringen, Germany). The mass spectrometer was operated in data-dependent acquisition mode, automatically switching between MS and MS2. Raw files were processed using MaxQuant (41) (versions 1.6.8.0 and 1.5.3.30 for TAP-ZC3H5 and co-immunoprecipitations, respectively) for peptide identification and quantification. MS2 spectra were searched against the *T. brucei* 927 annotated protein databases, (TriTrypDB release 46 and 8.1 for TAP-ZC3H5 and co-immunoprecipitations, respectively), contaminants of MaxQuant were included. We defined carbamidomethylation of cysteine residues as fixed modification and acetyl (protein N-term), oxidation of methionine, deamidation of aspartic and glutamic acid as variable modifications and trypsin/P as the proteolytic enzyme with up to two missed cleavages allowed. The maximum false discovery rate for proteins and peptides was 0.01, a minimum of two peptides per protein and a minimum peptide length of seven amino acids were required. Peptides shared between orthologues and paralogues were assigned to the same protein group. Analysis was done in LFQ mode. MaxQuant calculated individual mass tolerances for each peptide, with the initial mass tolerances of the precursor ion set to 20 and 4.5 ppm for the first and main searches, respectively. All other parameters are default parameters of MaxQuant.

Statistical analysis of the results was performed using the Perseus toolbox (version 1.6.2.1) (42). Proteins were filtered according to a minimum of two out of three valid values in one group. All missing values from this reduced matrix were replaced by background values from normal distribution (mean down shift = 0.3, S.D. down shift = 1.8). For statistical comparison, permutation-based FDR and Student's *t* test were used comparing the natural logarithm of the intensities from the experiments and the control groups. TAP-ERBP1 (7) or V5-ERBP1 (this work) were used as controls for TAP or V5 purifications, respectively. Significantly enriched proteins were selected (FDR = 0.01 or 0.05 for TAP-ZC3H5 or V5-co-immunoprecipitations, respectively).

RNA manipulation

Northern blots were probed with [^{32}P]-labeled DNA from ZC3H5, Tb927.7.3040, Tb927.11.10340, Tb927.2.4550, Tb927.3.1660, and tubulin genes. To identify the transcripts bound to ZC3H5, 2×10^9 cells were washed in ice-cold Voorheis' modified PBS (PBS supplemented with 10 mM glucose and 46 mM sucrose) and the cell pellet snap frozen in liquid nitrogen. The RNA immunoprecipitation was done essentially as described in Ref. 43. Briefly, the cell extracts were incubated with IgG-coupled magnetic beads (New England Biolabs) for 2 h at 4°C, and the flow-through (unbound) fraction was collected. After extensive washing, bound ZC3H5 was eluted using tobacco etch virus protease for 2 h at 16°C. RNA was isolated using TriFast reagent (Peqlab). Total RNA from the unbound fraction was depleted of rRNA using RNase H and a mixture of 50-base DNA oligos complementary to trypanosome rRNAs. The recovered RNA from both bound and unbound samples were then analyzed by RNA-Seq (David Ibberson, Bioquant). For transcriptome analysis, RNAi was induced with 250 ng.ml^{-1} tetracycline for either 9 or 12 h. Differences in mRNA abundance were assessed using DESeqU1 (44), a custom version of DESeq2 (45).

Immunofluorescence microscopy and FACS analysis

Immunofluorescence of bloodstream cells was performed as described previously (7). Primary antibodies were GFP 1:500 and tubulin 1:1000. Images were acquired using an Olympus IX81microscope and analyzed with Olympus xCellence Software or ImageJ. FACS analysis was performed as described (46).

Polysome fractionation and analysis

Polysome fractionation was performed according to Ref. 47. For each gradient, 5×10^8 cells were collected by centrifugation at 3000 rpm for 15 min. The cell pellet was resuspended in 50 ml serum-free medium and transferred to a 50-ml conical tube. The cells were then incubated with 100 μg/ml cycloheximide for 7 min at room temperature. Cells were pelleted again by centrifugation at 2300 rpm for 7 min at 4°C, washed with 1 ml ice-cold 1 × PBS and transferred to an Eppendorf tube. Cells were then lysed in 350 μl lysis buffer (20 mM Tris-HCl, pH 7.5, 20 mM KCl, 2 mM $MgCl_2$, 2 mM DTT, 1000 units RNasin RNase inhibitor (Promega), 10 μg/ml leupeptin, 0.2% IGEPAL, 200 mM sucrose, 100 μg/ml cycloheximide) and passed 15 times through the 21-gauge needle using a 1-ml syringe and then 15 times through the 27-gauge needle. The lysate was cleared by centrifugation at 15,000 × *g* for 10 min at 4°C in a microfuge. Salt concentration was adjusted to 120 mM KCl and the lysate was loaded on the 4 ml continuous linear 15–50% sucrose gradient. The gradients were centrifuged at 40,000 rpm for 2 h at 4°C in a SW 60 Ti swinging-bucket rotor (Beckman Coulter). Afterward, 16 fractions with a volume of 300 μl were collected by fractionation with the UV-visible detector (Teledyne Isco). For RNA purification, 900 μl TriFast was added to each tube and RNA was purified following manufacturer protocol. For each fraction, the reads for each ORF per million reads (RPM) were calculated. To be able to estimate the real distributions of each mRNA across the gradient, a small portion of each sequencing sample was subjected to Northern blotting, using a spliced leader probe to detect mRNA, and a human β-globin probe to check RNA yield after preparation and handling. The spliced leader signals were first corrected for RNA yield; then, we calculated the proportion of the total spliced leader signal that was in each fraction. The RPM values were multiplied by these values to obtain the representation in each fraction. To eliminate numbers after the decimal point, enabling analysis using in-house R scripts, all values were multiplied by 1000. Overall, the proportions (mean and S.D.) were free: 35 ± 4%; monosomes 24 ± 3%; light polysomes 24 ± 4%; and heavy polysomes 14 ± 3%. Some error is introduced by slight variations in the precise position of the boundaries, especially between light and heavy polysomes: the percentage in polysomes was 39 ± 3%.

Data availability

The MS data are available via ProteomeXchange with identifier PXD019073. ArrayExpress accession numbers for the RNA-Seq data are as follows: ZC3H5 RNAi, E-MTAB-9088; TAP-ZC3H5 pulldown, E-MTAB-9084; polysomes, E-MTAB-8069.

Acknowledgments—We thank Nina Papavisiliou for generously hosting K. B. during the latter part of this project. We also acknowledge Claudia Helbig and Ute Leibfried for technical support, David Ibberson of the BioQuant sequencing facility for cDNA library construction, and the Mass Spectrometry and Imaging facilities (Dr. Holger Lorenz) of the ZMBH.

Author contributions—K. B., C. C., and E. E. conceptualization; K. B., C. C., and E. E. data curation; K. B., K. L., C. C., and E. E. formal analysis; K. B. and E. E. validation; K. B., C. C., and E. E. investigation; K. B. and E. E. visualization; K. B., C. C., and E. E. writing-original draft; K. L. software; C. C. resources; C. C. funding acquisition; C. C. and E. E. writing-review and editing; E. E. supervision; E. E. methodology.

Funding and additional information—This work was supported by Deutsche Forschungsgemeinshaft Cl112/24 (to C. C.) and core support from the State of Baden-Württemberg.

Conflict of interest—The authors declare that they have no conflicts of interest with the contents of this article.

Abbreviations—The abbreviations used are: BF, bloodstream form; RBP, RNA-binding protein; DAPI, 4[prime],6-diamidino-2-phenylindole; FDR, false discovery rate; ANOVA, analysis of variance.

References

1. Clayton, C. (2019) Regulation of gene expression in trypanosomatids: Living with polycistronic transcription. *Open Biol.* **9,** 190072 CrossRef Medline
2. Erben, E. D., Fadda, A., Lueong, S., Hoheisel, J. D., and Clayton, C. (2014) A genome-wide tethering screen reveals novel potential post-transcriptional regulators in *Trypanosoma brucei*. *PLoS Pathog.* **10,** e1004178 CrossRef Medline
3. Lueong, S., Merce, C., Fischer, B., Hoheisel, J. D., and Erben, E. D. (2016) Gene expression regulatory networks in *Trypanosoma brucei*: Insights into the role of the mRNA-binding proteome. *Mol. Microbiol.* **100,** 457–471 CrossRef Medline
4. Castello, A., Horos, R., Strein, C., Fischer, B., Eichelbaum, K., Steinmetz, L. M., Krijgsveld, J., and Hentze, M. W. (2013) System-wide identification of RNA-binding proteins by interactome capture. *Nat. Protoc.* **8,** 491–500 CrossRef Medline
5. Dean, S., Sunter, J. D., and Wheeler, R. J. (2017) TrypTag.org: A trypanosome genome-wide protein localisation resource. *Trends Parasitol.* **33,** 80–82 CrossRef Medline
6. Alsford, S., Turner, D. J., Obado, S. O., Sanchez-Flores, A., Glover, L., Berriman, M., Hertz-Fowler, C., and Horn, D. (2011) High-throughput phenotyping using parallel sequencing of RNA interference targets in the African trypanosome. *Genome Res.* **21,** 915–924 CrossRef Medline
7. Bajak, K., Leiss, K., Clayton, C. E., and Erben, E. (2020) The endoplasmic reticulum-associated mRNA-binding proteins ERBP1 and ERBP2 interact in bloodstream-form *Trypanosoma brucei*. *PeerJ* **8,** e8388 CrossRef Medline
8. Lukeš, J., Skalický, T., Týč, J., Votýpka, J., and Yurchenko, V. (2014) Evolution of parasitism in kinetoplastid flagellates. *Mol. Biochem. Parasitol.* **195,** 115–122 CrossRef Medline
9. Fritz, M., Vanselow, J., Sauer, N., Lamer, S., Goos, C., Siegel, T. N., Subota, I., Schlosser, A., Carrington, M., and Kramer, S. (2015) Novel insights into RNP granules by employing the trypanosome's microtubule skeleton as a molecular sieve. *Nucleic Acids Res.* **43,** 8013–8032 CrossRef Medline
10. Anand, B., Verma, S. K., and Prakash, B. (2006) Structural stabilization of GTP-binding domains in circularly permuted GTPases: Implications for RNA binding. *Nucleic Acids Res.* **34,** 2196–2205 CrossRef Medline

11. Wittinghofer, A., and Vetter, I. R. (2011) Structure-function relationships of the G domain, a canonical switch motif. *Annu. Rev. Biochem.* **80,** 943–971 CrossRef Medline
12. Urbaniak, M. D., Martin, D. M., and Ferguson, M. A. (2013) Global quantitative SILAC phosphoproteomics reveals differential phosphorylation is widespread between the procyclic and bloodstream form lifecycle stages of *Trypanosoma brucei*. *J. Proteome Res.* **12,** 2233–2244 CrossRef Medline
13. Benz, C., and Urbaniak, M. D. (2019) Organising the cell cycle in the absence of transcriptional control: Dynamic phosphorylation co-ordinates the *Trypanosoma brucei* cell cycle post-transcriptionally. *PLoS Pathog.* **15,** e1008129 CrossRef Medline
14. Nascimento, L. M. D., Terrao, M., Marucha, K. K., Liu, B., Egler, F., and Clayton, C. (2020) The RNA-associated MKT1 and MKT1L form alternative PBP1-containing complexes in *Trypanosoma brucei*. *J. Biol. Chem.* **295,** 10940–10955 CrossRef Medline
15. Siegel, T. N., Hekstra, D. R., Wang, X., Dewell, S., and Cross, G. A. (2010) Genome-wide analysis of mRNA abundance in two life-cycle stages of *Trypanosoma brucei* and identification of splicing and polyadenylation sites. *Nucleic Acids Res.* **38,** 4946–4957 CrossRef Medline
16. Roditi, I., Furger, A., Ruepp, S., Schürch, N., and Bütikofer, P. (1998) Unravelling the procyclin coat of *Trypanosoma brucei*. *Mol. Biochem. Parasitol.* **91,** 117–130 CrossRef Medline
17. Koenig-Martin, E., Yamage, M., and Roditi, I. (1992) A procyclin-associated gene in *Trypanosoma brucei* encodes a polypeptide related to ESAG 6 and 7 proteins. *Mol. Biochem. Parasitol.* **55,** 135–145 CrossRef Medline
18. Brecht, M., and Parsons, M. (1998) Changes in polysome profiles accompany trypanosome development. *Mol. Biochem. Parasitol.* **97,** 189–198 CrossRef Medline
19. Helser, T. L., Baan, R. A., and Dahlberg, A. E. (1981) Characterization of a 40S ribosomal subunit complex in polyribosomes of *Saccharomyces cerevisiae* treated with cycloheximide. *Mol. Cell Biol.* **1,** 51–57 CrossRef Medline
20. Adams, C. C., Jakovljevic, J., Roman, J., Harnpicharnchai, P., and Woolford, J. L., Jr. (2002) *Saccharomyces cerevisiae* nucleolar protein Nop7p is necessary for biogenesis of 60S ribosomal subunits. *RNA* **8,** 150–165 CrossRef Medline
21. Jensen, B. C., Brekken, D. L., Randall, A. C., Kifer, C. T., and Parsons, M. (2005) Species specificity in ribosome biogenesis: A nonconserved phosphoprotein is required for formation of the large ribosomal subunit in *Trypanosoma brucei*. *Eukaryot. Cell* **4,** 30–35 CrossRef Medline
22. Prohaska, K., and Williams, N. (2009) Assembly of the *Trypanosoma brucei* 60S ribosomal subunit nuclear export complex requires trypanosome-specific proteins P34 and P37. *Eukaryot. Cell* **8,** 77–87 CrossRef Medline
23. Droll, D., Archer, S., Fenn, K., Delhi, P., Matthews, K., and Clayton, C. (2010) The trypanosome Pumilio-domain protein PUF7 associates with a nuclear cyclophilin and is involved in ribosomal RNA maturation. *FEBS Lett.* **584,** 1156–1162 CrossRef Medline
24. Mier, P., Pérez-Pulido, A. J., Reynaud, E. G., and Andrade-Navarro, M. A. (2017) Reading the evolution of compartmentalization in the ribosome assembly toolbox: The YRG protein family. *PLoS One* **12,** e0169750 CrossRef Medline
25. Thomson, E., Ferreira-Cerca, S., and Hurt, E. (2013) Eukaryotic ribosome biogenesis at a glance. *J. Cell Sci.* **126,** 4815–4821 CrossRef Medline
26. Heyer, E. E., and Moore, M. J. (2016) Redefining the translational status of 80S monosomes. *Cell* **164,** 757–769 CrossRef Medline
27. Kim, T. S., Kim, H. D., Park, Y. J., Kong, E., Yang, H. W., Jung, Y., Kim, Y., and Kim, J. (2019) JNK activation induced by ribotoxic stress is initiated from 80S monosomes but not polysomes. *BMB Rep.* **52,** 502–507 CrossRef Medline
28. Bécam, A. M., Nasr, F., Racki, W. J., Zagulski, M., and Herbert, C. J. (2001) Ria1p (Ynl163c), a protein similar to elongation factors 2, is involved in the biogenesis of the 60S subunit of the ribosome in *Saccharomyces cerevisiae*. *Mol. Genet. Genomics* **266,** 454–462 CrossRef Medline
29. Baierlein, C., Hackmann, A., Gross, T., Henker, L., Hinz, F., and Krebber, H. (2013) Monosome formation during translation initiation requires the serine/arginine-rich protein Npl3. *Mol. Cell Biol.* **33,** 4811–4823 CrossRef Medline
30. Jaremko, D., Ciganda, M., Christen, L., and Williams, N. (2019) *Trypanosoma brucei* L11 is essential to ribosome biogenesis and interacts with the kinetoplastid-specific proteins P34 and P37. *mSphere* **4,** e00475-19 CrossRef Medline
31. Kim, S. J., and Strich, R. (2016) Rpl22 is required for IME1 mRNA translation and meiotic induction in *S. cerevisiae*. *Cell Div.* **11,** 10 CrossRef Medline
32. de Freitas Nascimento, J., Kelly, S., Sunter, J., and Carrington, M. (2018) Codon choice directs constitutive mRNA levels in trypanosomes. *Elife* **7,** e32467 CrossRef Medline
33. Yu, H., Dee, D. R., Liu, X., Brigley, A. M., Sosova, I., and Woodside, M. T. (2015) Protein misfolding occurs by slow diffusion across multiple barriers in a rough energy landscape. *Proc. Natl. Acad. Sci. U. S. A.* **112,** 8308–8313 CrossRef Medline
34. Park, H., and Subramaniam, A. R. (2019) Inverted translational control of eukaryotic gene expression by ribosome collisions. *PLos Biol.* **17,** e3000396 CrossRef Medline
35. Redmond, S., Vadivelu, J., and Field, M. C. (2003) RNAit: An automated web-based tool for the selection of RNAi targets in *Trypanosoma brucei*. *Mol. Biochem. Parasitol.* **128,** 115–118 CrossRef Medline
36. Jones, N. G., Thomas, E. B., Brown, E., Dickens, N. J., Hammarton, T. C., and Mottram, J. C. (2014) Regulators of *Trypanosoma brucei* cell cycle progression and differentiation identified using a kinome-wide RNAi screen. *PLoS Pathog.* **10,** e1003886 CrossRef Medline
37. Maier, R., Brandner, C., Hintner, H., Bauer, J., and Onder, K. (2008) Construction of a reading frame-independent yeast two-hybrid vector system for site-specific recombinational cloning and protein interaction screening. *BioTechniques* **45,** 235–244 CrossRef Medline
38. Mugo, E., and Erben, E. D. (2020) The tethering assay: A simple method for the characterization of mRNA-fate regulators. *Methods Mol. Biol.* **2116,** 295–301 CrossRef Medline
39. Singh, A., Minia, I., Droll, D., Fadda, A., Clayton, C., and Erben, E. (2014) Trypanosome MKT1 and the RNA-binding protein ZC3H11: Interactions and potential roles in post-transcriptional regulatory networks. *Nucleic Acids Res.* **42,** 4652–4668 CrossRef Medline
40. Mugo, E., and Clayton, C. (2017) Expression of the RNA-binding protein RBP10 promotes the bloodstream-form differentiation state in *Trypanosoma brucei*. *PLoS Pathog.* **13,** e1006560 CrossRef Medline
41. Cox, J., and Mann, M. (2008) MaxQuant enables high peptide identification rates, individualized p.p.b.-range mass accuracies and proteome-wide protein quantification. *Nat. Biotechnol.* **26,** 1367–1372 CrossRef Medline
42. Tyanova, S., Temu, T., Sinitcyn, P., Carlson, A., Hein, M. Y., Geiger, T., Mann, M., and Cox, J. (2016) The Perseus computational platform for comprehensive analysis of (prote)omics data. *Nat. Methods* **13,** 731–740 CrossRef Medline
43. Mugo, E., and Erben, E. D. (2020) Identifying trypanosome protein-RNA interactions using RIP-Seq. *Methods Mol. Biol.* **2116,** 285–294 CrossRef Medline
44. Leiss, K. (2017) klprint/DESeqUI: DESeqUI 1.0.2. *Zenodo* CrossRef
45. Love, M. I., Huber, W., and Anders, S. (2014) Moderated estimation of fold change and dispersion for RNA-Seq data with DESeq2. *Genome Biol.* **15,** 550 CrossRef Medline
46. Archer, S. K., Inchaustegui, D., Queiroz, R., and Clayton, C. (2011) The cell cycle regulated transcriptome of *Trypanosoma brucei*. *PLoS One* **6,** e18425 CrossRef Medline
47. Bajak, K., and Clayton, C. (2020) Polysome profiling and metabolic labeling methods to measure translation in *Trypanosoma brucei*. *Methods Mol. Biol.* **2116,** 99–108 CrossRef Medline
48. Fadda, A., Ryten, M., Droll, D., Rojas, F., Färber, V., Haanstra, J. R., Merce, C., Bakker, B. M., Matthews, K., and Clayton, C. (2014) Transcriptome-wide analysis of trypanosome mRNA decay reveals complex degradation kinetics and suggests a role for co-transcriptional

degradation in determining mRNA levels. *Mol Microbiol*. **94,** 307–326 CrossRef Medline

49. Antwi, E. B., Haanstra, J. R., Ramasamy, G., Jensen, B., Droll, D., Rojas, F., Minia, I., Terrao, M., Mercé, C., Matthews, K., Myler, P. J., Parsons, M., and Clayton, C. (2016) Integrative analysis of the Trypanosoma brucei gene expression cascade predicts differential regulation of mRNA processing and unusual control of ribosomal protein expression. *BMC Genomics*. **17,** 306 CrossRef Medline
50. Flegontov, P., Votýpka, J., Skalický, T., Logacheva, M. D., Penin, A. A., Tanifuji, G., Onodera, N. T., Kondrashov, A. S., Volf, P., Archibald, J. M., and Lukeš, J. (2013) Paratrypanosoma is a novel early-branching trypanosomatid. *Curr. Biol*. **23,** 1787–1793 CrossRef Medline
51. Silvester, E., Ivens, A., and Matthews, K. R. (2018) A gene expression comparison of *Trypanosoma brucei* and *Trypanosoma congolense* in the bloodstream of the mammalian host reveals species-specific adaptations to density-dependent development. *PLoS Negl. Trop. Dis*. **12,** e0006863 CrossRef Medline